

Asteroseismological studies of three β Cephei stars: IL Vel, V433 Car and KZ Mus

G. Handler^{1,2}, R. R. Shobbrook³, F. F. Vuthela^{2,4}, L. A. Balona², F. Rodler¹,
T. Tshenye⁴

¹ *Institut für Astronomie, Universität Wien, Türkenschanzstraße 17, A-1180 Wien, Austria*

² *South African Astronomical Observatory, P.O. Box 9, Observatory 7935, South Africa*

³ *Visiting Fellow, Australian National University, Canberra, ACT, Australia*

⁴ *Department of Physics, University of the North-West, Private Bag X2046, Mmabatho 2735, South Africa*

Accepted 2003 nnnn nn. Received 2002 nnnn nn; in original form 2002 nnnn nn

ABSTRACT

We have acquired between 127 and 150 h of time-resolved multicolour photometry for each of the three β Cephei stars IL Vel, V433 Car and KZ Mus over a time span of four months from two observatories. All three objects are multiperiodic with at least three modes of pulsation.

Mode identification from the relative colour amplitudes is performed. We obtain unambiguous results for the two highest-amplitude modes of IL Vel (both are $\ell = 1$) and the three strongest modes of KZ Mus ($\ell = 2, 0$ and 1), but none for V433 Car. Spectroscopy shows the latter star to be a fast rotator ($v \sin i = 240$ km/s), whereas the other two have moderate $v \sin i$ (65 and 47 km/s, respectively).

We performed model calculations with the Warsaw-New Jersey stellar evolution and pulsation code. We find that IL Vel is an object of about $12 M_{\odot}$ in the second half of its main sequence evolutionary track. Its two dipole modes are most likely rotationally split components of the mode originating as p_1 on the ZAMS; one of these modes is $m = 0$. V433 Car is suggested to be an unevolved $13 M_{\odot}$ star just entering the β Cephei instability strip. KZ Mus seems less massive ($\approx 12.7 M_{\odot}$) and somewhat more evolved, and its radial mode is probably the fundamental one. In this case its quadrupole mode would be the one originating as g_1 , and its dipole mode would be p_1 .

Two of our photometric comparison stars also turned out to be variable. HD 90434 is probably a new slowly pulsating B star whose dominant mode is a dipole, whereas the variability of HD 89768 seems to be due to binarity.

It is suggested that mode identification of slowly rotating β Cephei stars based on photometric colour amplitudes is reliable; we estimate that a relative accuracy of 3% in the amplitudes is sufficient for unambiguous identifications. Due to the good agreement of our theoretical and observational results we conclude that the prospects for asteroseismology of multiperiodic slowly rotating β Cephei star are good.

Key words: stars: variables: other – stars: early-type – stars: oscillations – stars: individual: IL Vel – stars: individual: V433 Car – stars: individual: KZ Mus – techniques: photometric

1 INTRODUCTION

The β Cephei stars are a group of early B-type stars of luminosity classes III–V that pulsate in pressure (p) and gravity (g) modes of low radial overtone. Their pulsational behaviour is thus similar to that of the A/F-type δ Scuti stars.

Both classes of variable seem suitable for asteroseismological investigations: their pulsational frequencies may be used to sound their interiors as the associated modes penetrate deeply into the star.

As exciting as this possibility is in theory, practice has

shown that several obstacles still need to be overcome before precision asteroseismology of β Cephei or δ Scuti stars can be done. On the theoretical side an adequate description of higher-order rotational effects is being worked on (e.g. Soufi, Goupil & Dziembowski 1998), and mode coupling is expected to have major effects on the pulsational eigenspectra of fast rotators (see Daszyńska-Daszkiewicz et al. 2002). Observationally, the main problem is the detection and identification of as many pulsation modes as possible because a complete set of mode spectra has not even nearly been detected for any of these pulsators.

It may be suspected that the δ Scuti stars offer better possibilities for asteroseismology than β Cephei stars do, as they generally have many more pulsation modes excited to observable amplitudes. This result is in agreement with theoretical investigations of mode excitation (e.g. Pamyatnykh 2003). However, the problem lies with mode identification, that is, the match of the observed frequencies with the corresponding pulsation mode defined by the three parameters k , the radial overtone of the mode, the spherical degree ℓ and the azimuthal order m .

To accomplish such a match in the presence of incomplete observed pulsation spectra, it is necessary to use mode identification methods. However, the surface convection zones of δ Scuti stars are expected to affect some of these methods, like the commonly used photometric method that utilises and amplitude ratios and/or phase shifts of the light curves in different filters, adversely (see Balona & Evers 1999), and it is not known if they can be trusted. The β Cephei stars do not have surface convection zones and therefore the simple photometric method may be applicable with more confidence.

We have therefore chosen three β Cephei stars whose literature data qualify them as interesting candidates for in-depth studies aiming at the detection of many pulsation frequencies and at their mode identification by photometric means. All these objects have been reported as multiperiodic variables before and photometric mode identifications have been attempted. However, in all cases the amount of data available was small enough to give us hope for a significant improvement over previous results if we can obtain $\gtrsim 100$ h of observation.

The most comprehensive photometric study of IL Vel (HD 80383) was performed by Heynderickx & Haug (1994). They found four frequencies in their UVB light curves, three of which formed an equally spaced triplet, suggestive of rotational m -mode splitting. This frequency solution did however not fit additional data in the Walraven system within the precision of the measurements. Heynderickx, Waelkens & Smeyers (1994) used the Walraven data for mode identification and suggested that all modes are of degree $\ell = 0$ and $\ell = 1$.

The variability of V433 Car (HD 90288) was discovered by Lampens (1988) and followed up by Heynderickx (1992). The frequency analysis of all the Geneva and Walraven data available to Heynderickx (1992) allowed him to disentangle four frequencies in the light variations of V433 Car. The mode identification by Heynderickx et al. (1994) was somewhat ambiguous, but suggested a mixture of (possibly) radial and nonradial modes with spherical degrees ℓ up to 4.

Our third target star, KZ Mus (HD 109885) was a dis-

covery of the HIPPARCOS satellite (ESA 1997) reported by Waelkens et al. (1998). Aerts (2000) obtained new Geneva photometry for the star and performed both a frequency analysis of all data and mode identification. She suggested that the star pulsates with at least three frequencies, where the second strongest one appeared to be radial.

2 OBSERVATIONS

2.1 Photometry

We have studied IL Vel, V433 Car and KZ Mus from both the Siding Spring (SSO, Australia) and South African Astronomical (SAAO) Observatories. We used photoelectric photometers attached to the 0.6-m telescope at SSO and the 0.5-m and 0.75-m telescopes at SAAO.

The most valuable part of the energy distribution of a β Cephei star for mode identification by means of photometry is in the blue ($\lambda < 4200$ Å). Therefore, the Geneva and (particularly) Walraven systems are well suited for such a purpose as they have several filters in this wavelength domain. Unfortunately, these are not widely available. Owing to the faintness of our variables ($V = 8.1 - 9.1$) we decided to utilise the standard Johnson UVB system, supplemented by Strömgren v whenever possible.

The periods of the known pulsations of our three targets are all longer than 150 minutes, and the stars are all located in an area covering some 30° on the sky. Consequently, we chose one local comparison star for each variable (the B5 IV star HD 79670 for IL Vel, the B9 IV/V star HD 90434 that was later replaced by the A1 IV/V star HD 89768 for V433 Car and the B9 IV star HD 109082 for KZ Mus; all spectral types are from Houk & Cowley 1975), and our observing sequence included all six stars whenever reachable. The resulting cycle time of about 25 minutes (or less) per measurement of each variable sampled the light curves of all stars adequately.

Another aspect of the pulsations of β Cephei stars requires consideration when planning an observational effort such as ours. In many cases, closely spaced pulsation frequencies are present. As mentioned above Heynderickx & Haug (1994) reported just that for our target IL Vel. Consequently, a sufficient time baseline must be spanned by the observations (at least 2 months for IL Vel) for such frequencies to be resolved and the measurements should be distributed evenly over the observation period to avoid aliasing problems.

We have therefore also observed these objects during a multisite campaign for the δ Scuti star FG Vir (Breger et al., in preparation) when this star was not reachable. This only resulted in short runs up to two hours that however covered important gaps in the total coverage which made them quite valuable. The main body of our final data set spanned 94 days in February to May 2002, during which data was obtained on 52 nights. A total of 146 hr of measurement of IL Vel, 150 hr of V433 Car and 127 hr of KZ Mus was acquired.

Data reduction was performed in the standard way for differential photoelectric time-series photometry. First, we corrected the data for coincidence losses, followed by sky subtraction and by extinction determination using the time

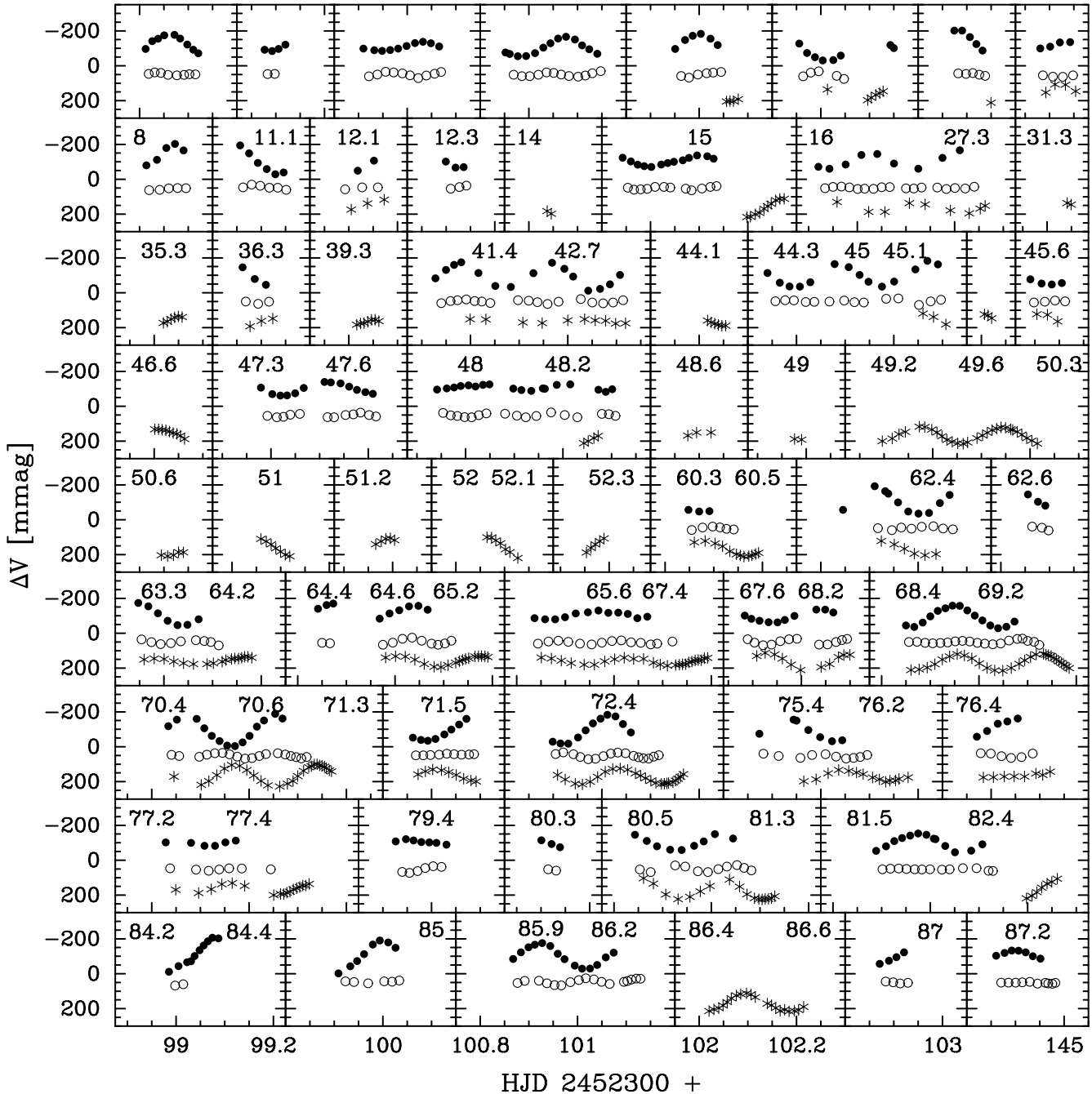


Figure 1. V-filter light curves from all our measurements of IL Vel (filled circles), V433 Car (open circles) and KZ Mus (asterisks). Note the shorter periods and much lower amplitude of V433 Car. Multiperiodicity of all three stars is evident.

series of the constant stars in our ensemble. After the extinction correction, the differential light curves of the variables with respect to their local comparison stars and that of the three comparison with respect to the others were calculated and the times of measurement were converted to Heliocentric Julian Date (HJD). The light curves of the three β Cephei stars in the V filter are shown in Fig. 1.

As part of the reductions were already performed during the observational campaign, it was noticed that the comparison star HD 90434 was variable. Consequently, it was replaced by HD 89768. As it turned out during the final

reductions after completion of the observations, this star is also variable. We will analyse these objects later, but for the time being let it suffice to say that we performed a frequency analysis of their differential light curves with respect to the constant comparison stars for the other targets. We then subtracted synthetic light curves built from the results of this frequency search from the differential measurements of V433 Car so the variability of its comparison stars will not affect the frequency analysis of this star. This procedure is valid as the time scales of the variability of HD 90434 and HD 89768 is much longer than that of V433 Car.

Table 1. Results of our determinations of the radial and projected rotational velocities.

Star	$v \sin i$ [km/s]	$\langle Vr \rangle$ [km/s]
IL Vel	65 ± 3	+19.0
V433 Car	240 ± 10	+4.0
KZ Mus	47 ± 3	-61.6

2.2 Spectroscopy

With the main aim of determining the projected rotational velocities of IL Vel, V433 Car and KZ Mus, high-resolution spectra of the three β Cephei stars were obtained on the night of 4/5 May 2002 with the 1.9-m telescope at SAAO. We used the **GIRAFFE** echelle fibre-fed spectrograph attached to the Cassegrain focus of this telescope. The **GIRAFFE** spectrograph has a resolving power of about 32 000, giving a resolution of 0.06 – 0.09 Å per pixel. Exposure times were 1500 seconds for IL Vel and KZ Mus as well as 600 seconds for V433 Car for 7S/N ratios between 27 and 35. A Th-Ar arc lamp was used for wavelength calibration.

The spectra were normalised to the continuum by using an unbroadened synthetic spectrum with $T_{\text{eff}} = 23000$ K, $\log g = 4.00$ as a template, using the **SPECTRUM** code (Gray & Corbally 1994). A running median of each echelle order was divided by the corresponding section of the synthetic spectrum and taken to represent the response function of the instrument. A polynomial of degree 5 was fitted to the response function and used to correct the observed spectrum.

For each order, the observed rectified spectrum was correlated with the corresponding section of the synthetic spectrum after removing the unit continuum, effectively resulting in the mean line profile with the continuum removed. A quadratic was then fitted to the correlation function, and its maximum adopted as the “radial velocity” for each order. The mean radial velocity from all the orders is also obtained.

The correlation profiles can be co-added to form what is essentially a mean line profile. The projected rotational velocity, $v \sin i$, can be determined by fitting a model profile of a rotating star. The projected rotational velocity is adjusted until a best fit is obtained to the observed profile. We show these fits in Fig. 2; the results from our spectroscopic analysis are summarised in Table 1.

3 FREQUENCY ANALYSIS OF THE PHOTOMETRIC TIME SERIES

Our frequency analysis was performed with the program **PERIOD 98** (Sperl 1998). This package applies single-frequency power spectrum analysis and simultaneous multi-frequency sine-wave fitting. One of its many advanced features is its capability to fix dependent signal frequencies to certain values, e.g. to sum and difference terms, and to perform simultaneous nonlinear least squares fits with such fixed frequencies.

Our strategy for the frequency analysis starts with the calculation of the spectral window of the data. It is computed as the Fourier amplitude spectrum of a single noise-free sine wave with the frequency of highest amplitude in

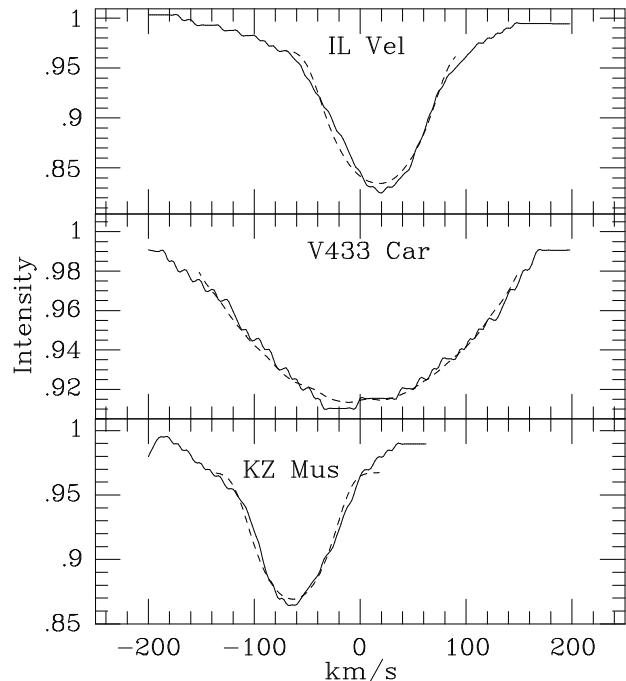


Figure 2. The average Helium line profile for our three variables (full line) overlaid by a model atmosphere fit (dashed lines) to determine the projected rotational velocities. The line profile asymmetries are likely caused by nonradial stellar pulsation.

our data. In this way, the reflection of the spectral window pattern at zero frequency, which may not be negligible as our observing nights often did not sample a full cycle of the light variations, can be evaluated.

We continue by computing amplitude spectra of our data as well as those of residual light curves after the previously identified periodicities had been removed using the multi-periodic fitting algorithm of **PERIOD 98**. We continue this process until no significant peaks are left in the residual amplitude spectrum. We consider an independent peak significant if it exceeds four times the local noise level in the amplitude spectrum, following Breger et al. (1993). Combination signals only require $S/N > 3.5$ to be regarded as significant. Experience has shown that this criterion is both reliable and conservative.

Similar analyses were performed for all the four filters used. We note that, within the uncertainties of frequency determination, these detected frequencies were the same for all stars in every filter. This confirms that alias ambiguities do not affect our analysis. As our final values for the frequencies we adopted the mean values from the data in all four filters weighted by the associated signal-to-noise ratios. The deviations of the optimum frequencies in the individual filters from this mean is taken as our error estimate on the frequency determination.

3.1 KZ Mus

As the frequency analysis of this star was straightforward, it is the first that we chose to describe. The spectral window, amplitude spectra, and prewhitened versions thereof are shown in Fig. 3. We use the data obtained in the B filter

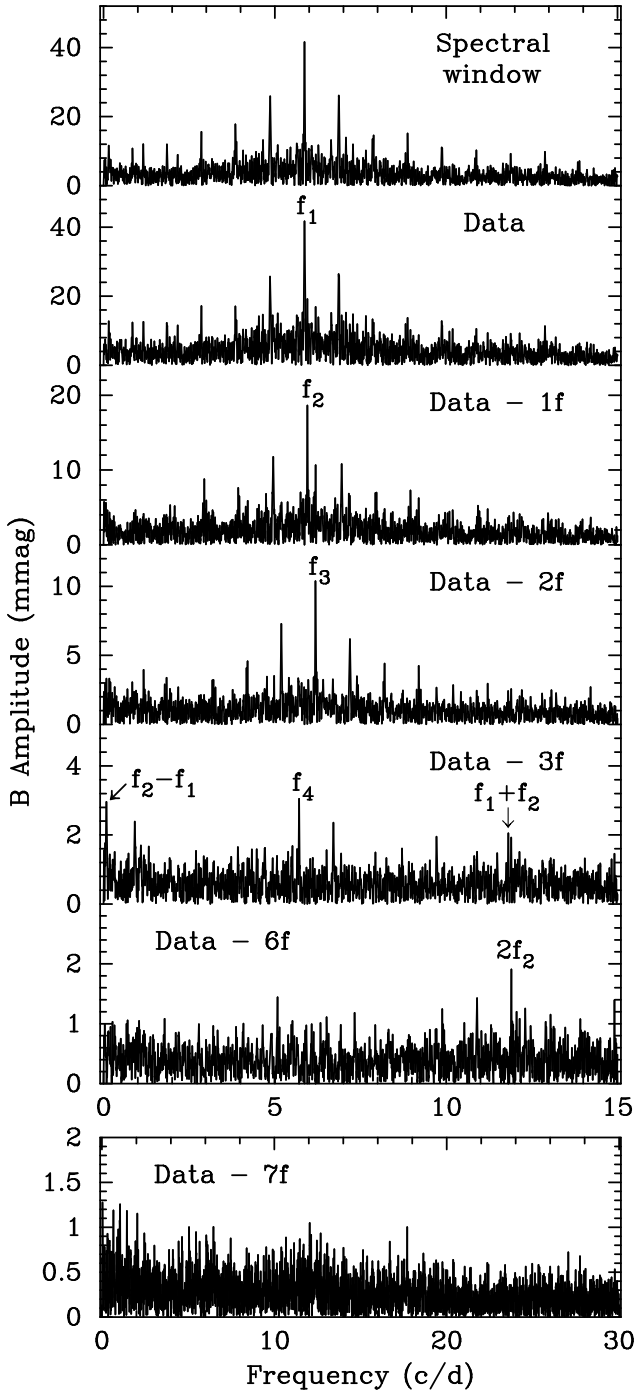


Figure 3. Spectral window and amplitude spectra of our B filter data of KZ Mus. Some prewhitening steps of the detected frequencies are shown in consecutive panels. The lowest panel shows the amplitude spectrum of the combined UvBV residuals after all significant signals have been removed from the measurements.

for display as they have best S/N ratio. Due to our two-site coverage the spectral window is sufficiently clean so that alias ambiguities do not represent a problem for the analysis.

The first three signals in the periodogram are easy to detect. After prewhitening these, a more complicated residual amplitude spectrum (fifth panel of Fig. 3), with several

peaks standing out, remains. A closer look reveals that two of them are the combination sum and difference frequencies of the two strongest modes, whereas the remaining tall peak corresponds to an independent signal. Prewhitening all the six variations detected so far, the $2f$ -harmonic of the second strongest mode also becomes notable.

After this signal is included in our multifrequency light-curve fit, no significant peaks remain in the residual amplitude spectrum of the B filter data alone, and neither are there any present in the measurements in any other filter. However, we can attempt to increase the signal to noise in our analysis by adding the data in all filters. Obviously, this must not be done for the original light curves, as different pulsation modes have different relative amplitudes in the different wavelength passbands (that are a diagnostic for mode identification!). It is however safe to combine the residual light curves as we are working at low S/N ratio, i.e. the intrinsic differences in mode amplitude between the wavebands are small compared to the noise in the data.

To combine the different residual data sets we have therefore subtracted a multifrequency solution from all the individual filters' observations, using exactly the same frequencies (determined as described in the previous section) for each waveband. We then roughly scaled the residuals to B amplitude by multiplying the U filter residuals by 0.8 and the V filter residuals by 1.1. We did not scale the v filter data as the signals in it were found to have essentially the same amplitude as in B. The scale factors are approximate average amplitude ratios of the modes previously detected.

All these residual light curves were then added together, averaged, and the periodogram was computed out to the Nyquist frequency (lowest panel of Fig. 3); we find no more significant signals. Interestingly, we do note two residual mounds of amplitude, one in the frequency region where the pulsational signals were found and another one where combination frequencies would be expected. In fact, the two highest peaks in the latter region are located at exact sums of two known frequencies but they are not formally significant.

We can therefore claim the detection of seven signals in the light curves of KZ Mus; our final frequency solution is listed in Table 2. The rms scatter per single data point in the combined and averaged UvBV residuals is 3.0 mmag.

3.1.1 Re-analysis of published data

Our frequency solution in Table 2 differs somewhat from the results of Aerts (2000), who needed to base her frequency analysis on the HIPPARCOS data of the star. The first two signals detected by her agree with ours, but the third one is different; the remaining signals are below her detection level. Two possible reasons for the disagreement can be imagined, the more exciting one being intrinsic amplitude variability of the star and the other one being an alias problem in the poorly sampled HIPPARCOS photometry.

Consequently, we have re-analysed the time series of KZ Mus acquired by the HIPPARCOS satellite. The residual amplitude spectrum after prewhitening the two consistent main frequencies contains the third signal claimed by Aerts (2000) as the tallest peak. However, our third signal is also visible and of similar strength. As our data are more extensive and of better quality than the HIPPARCOS pho-

Table 2. Multifrequency solution for our KZ Mus data. Frequencies are mean values from results of all four filters weighted by the S/N ratio of the signal. Errors on the amplitudes were calculated with the formulae of Montgomery & O’Donoghue (1999). The S/N ratio quoted is the average of the values in the individual filters.

ID	Frequency (c/d)	Amplitude				mean S/N
		U (mmag)	B (mmag)	V (mmag)	v (mmag)	
f_1	5.86384 ± 0.00006	45.6 ± 0.3	40.9 ± 0.3	38.5 ± 0.3	41.2 ± 0.4	89.4
f_2	5.95026 ± 0.00011	28.8 ± 0.3	19.6 ± 0.3	16.4 ± 0.3	20.6 ± 0.4	45.6
f_3	6.1874 ± 0.0005	14.3 ± 0.3	11.0 ± 0.3	10.5 ± 0.3	11.8 ± 0.4	25.7
f_4	5.7090 ± 0.0024	3.4 ± 0.3	3.2 ± 0.3	2.4 ± 0.3	3.1 ± 0.4	6.6
$f_2 - f_1$	0.08642	4.3 ± 0.3	2.8 ± 0.3	3.1 ± 0.3	3.1 ± 0.4	6.3
$f_1 + f_2$	11.81410	2.5 ± 0.3	2.2 ± 0.3	2.5 ± 0.3	2.6 ± 0.4	5.7
$2f_2$	11.90052	2.6 ± 0.3	1.9 ± 0.3	2.0 ± 0.3	2.6 ± 0.4	5.2

tometry, we suggest that the third signal found by Aerts (2000) is an unfortunate artifact of the poor sampling of the HIPPARCOS measurements.

3.2 V433 Car

The upper panel of Fig. 4 shows that the spectral window function for our measurements of this star is also quite good. The amplitude spectrum is dominated by two peaks of similar strength that seem to imply an aliasing problem, but thanks to the long time base of our data they are well resolved and do not interfere with each other; they are simply two independent signals of similar amplitude.

Prewhitening of these variations results in the detection of a third frequency and the next step reveals another significant peak. After these four periodicities have been removed, no obvious new candidate frequency can be discerned. We therefore combined the residual data as we did for KZ Mus, but used somewhat different scale factors that seemed more appropriate for this star. We multiplied the U residuals by 0.83 and the ones in V by 1.05 to obtain approximate B amplitudes.

The amplitude spectrum of the residuals thus combined is shown in the lowest panel of Fig. 4, again out to the Nyquist frequency. The highest peak corresponds to a combination frequency difference and as it exceeds the noise level more than 3.5 times, we adopt it as an additional term for our frequency solution. We would also like to point out the peak near 7 c/d in the lowest panel of Fig. 4. It is in fact a close doublet at 6.924 and 6.968 c/d that is present in the residuals of all individual filters, but as it still does not exceed $S/N > 4$, we cannot be sure about its reality. We therefore adopt a five-frequency solution for our light curves that we list in Table 3.

The rms scatter of the combined residual light curves of V433 Car is 3.9 mmag per point. This is 30% higher than for KZ Mus. Likely reasons for the increased noise are undetected further intrinsic signals and possible residual variations by the variable comparison stars that could not be taken out.

3.2.1 Comparison with literature data

Heynderickx (1992) reported the detection of four frequencies in his light curves of V433 Car. Two of them agree with the two strongest signals in our Table 3, and the other two

are 1 c/d aliases of our values. We prefer the frequencies derived our analysis because our data are more numerous, the results in the different filters were consistent and as our two-site measurements have a much better spectral window function.

The order in which we detected the variation frequencies of V433 Car is different from the one obtained by Heynderickx (1992). Although this author does not list the amplitudes of the signals he determined, inspection of his published PDM periodograms suggests that the pulsations suffered amplitude variability in the 14 years that have elapsed between his and our observations.

3.3 IL Vel

The spectral window and amplitude spectra of our measurements of IL Vel are shown in Fig. 5. Two independent frequencies dominate the periodogram. After prewhitening those, a third signal stands out, and including that one in the multifrequency solution allows the detection of two combinations frequencies. Combining the residuals in all filters, scaling the U data by a factor of 0.76 and the V data by 1.05, results in the uninformative periodogram in the lowest panel of Fig. 5. The frequency solution for IL Vel is given in Table 4.

This analysis may appear simple, but it is not. Firstly, the third independent signal is located halfway between the first two that are of much higher amplitude. Although it is well resolved from the two strong modes, some doubts remain as to its reality; it could be an artifact caused by amplitude/frequency variability of the two main signals.

We have therefore divided our data set into two halves (before and after JD 2452360) and analysed them separately. We adopted the frequencies of the two strongest modes and their detected combination signals as definite and fitted them to each half, but left their amplitudes and phases as free parameters. We then computed amplitude spectra of the residuals for each half in each filter. The signal f_3 was detected in each of the 8 subsets of data; we conclude that it is real.

The second cause of concern is the rms residual of our five-frequency fit to the IL Vel light curves. After combination of the data in all four filters, it is an enormous 7.8 mmag per point, twice as large as for V433 Car and 2.6 times larger than for KZ Mus. The noise level in the lowest panel of Fig. 5 is also correspondingly higher.

Table 3. Multifrequency solution for our V433 Car data. Frequencies are mean values from results of all four filters weighted by the S/N ratio of the signal. Errors on the amplitudes were calculated with the formulae of Montgomery & O’Donoghue (1999). The S/N ratio quoted is the average of the values in the individual filters.

ID	Frequency (c/d)	Amplitude				mean S/N
		U (mmag)	B (mmag)	V (mmag)	v (mmag)	
f_1	9.12909 ± 0.00014	9.9 ± 0.5	8.2 ± 0.3	8.2 ± 0.3	8.8 ± 0.5	17.9
f_2	8.31649 ± 0.00009	10.0 ± 0.5	8.2 ± 0.3	7.3 ± 0.3	8.0 ± 0.5	16.7
f_3	9.66707 ± 0.00024	4.3 ± 0.5	3.8 ± 0.3	4.0 ± 0.3	4.2 ± 0.5	8.5
f_4	7.7214 ± 0.0012	3.4 ± 0.5	2.8 ± 0.3	2.3 ± 0.3	2.6 ± 0.5	5.4
$f_3 - f_1$	0.53798	1.8 ± 0.5	1.2 ± 0.3	1.5 ± 0.3	1.3 ± 0.5	3.7

Table 4. Multifrequency solution for our IL Vel data. Frequencies are mean values from results of all four filters weighted by the S/N ratio of the signal. Errors on the amplitudes were calculated with the formulae of Montgomery & O’Donoghue (1999). The S/N ratio quoted is the average of the values in the individual filters.

ID	Frequency (c/d)	Amplitude				mean S/N
		U (mmag)	B (mmag)	V (mmag)	v (mmag)	
f_1	5.45976 ± 0.00012	59.9 ± 0.8	45.5 ± 0.6	43.2 ± 0.7	45.6 ± 0.7	43.2
f_2	5.36293 ± 0.00011	53.0 ± 0.8	40.7 ± 0.6	38.3 ± 0.7	40.6 ± 0.7	38.4
f_3	5.41340 ± 0.0010	8.7 ± 0.8	7.1 ± 0.6	6.5 ± 0.7	7.3 ± 0.7	6.6
$f_1 + f_2$	10.82269	5.2 ± 0.8	4.0 ± 0.6	4.1 ± 0.7	3.7 ± 0.7	4.2
$f_2 - f_1$	0.09683	5.3 ± 0.8	3.3 ± 0.6	3.4 ± 0.7	4.4 ± 0.7	3.7

We started our quest for the reason for the high residuals by investigating the constancy of the comparison star. We calculated differential light curves to all the other stars that we had simultaneous data for, but found no evidence for variability of HD 79670, at least at a level that could produce the high residuals observed. They must therefore be (mostly) due to IL Vel.

When we checked the reality of f_3 , we noted that its location in the amplitude spectra of the two subsets of data was somewhat shifted and that there was more structure surrounding it than just the normal spectral window pattern plus noise. A plot of the residual light curves after subtraction of our five-frequency solution shows conspicuous variability on time scales similar to those of the known pulsational signals. We are therefore inclined to think that further, presently unresolved, pulsation frequencies are present in the light curves of IL Vel and that a data set with an even longer time base than ours is required to detect them.

3.3.1 Re-analysis of published data

The results of our frequency analysis differ from that by Heynderickx & Haug (1994). Our first frequency is significantly different from theirs, but we agree on the second one. Heynderickx & Haug (1994) did not find our third frequency, whereas we did not detect their third and fourth signals.

To clarify the situation, we have retrieved the data by Heynderickx & Haug (1994) and re-analysed them. We show the periodogram analysis of their Johnson B data in Fig. 6, where we have assumed our frequencies to be correct, and used them as the initial values for light curve-fitting and prewhitening.

Our two frequencies f_1 and f_2 are sufficient to explain the dominant variations in these measurements. Af-

ter they are prewhitened, the residual amplitude spectrum (lowest panel of Fig. 6) shows no peak exceeding 5 mmag; the two additional frequencies claimed by Heynderickx & Haug (1994) had B amplitudes of 20 and 14 mmag, respectively. We conclude that these were artifacts originating from choosing a wrong alias frequency.

The absence of our signal f_3 in their data may be due to a similar reason. Two out of their three yearly data sets spanned two weeks, and one consisted two single-week runs spread by 25 days. The beating phenomenon of f_3 with either f_1 or f_2 is therefore never properly resolved. Due to this particular unfortunate time distribution f_3 can be suppressed below detectability, as we have checked with numerical simulations. It is therefore well possible that our f_3 was present in their data but could not be detected. We note that the two combination frequencies detected in our data may also be present in the measurements by Heynderickx & Haug (1994), but if so, their amplitude was lower.

Finally, we would like to point out that the lowest panel of Fig. 6 also shows a residual mound of power, even more pronounced than in the residual periodogram of our data. The combined, scaled and average UBv residuals of the data by Heynderickx & Haug (1994) have an rms scatter of 9.8 mmag, also much higher than their measurement accuracy. As these authors used a comparison star different from ours, we strengthen the conclusion that there are unresolved frequencies in the light curves of IL Vel.

3.4 Variable comparison stars

3.4.1 HD 90434

This was the original local comparison star for V433 Car. When we examined amplitude spectra of the differential data reduced during the course of the observing campaign,

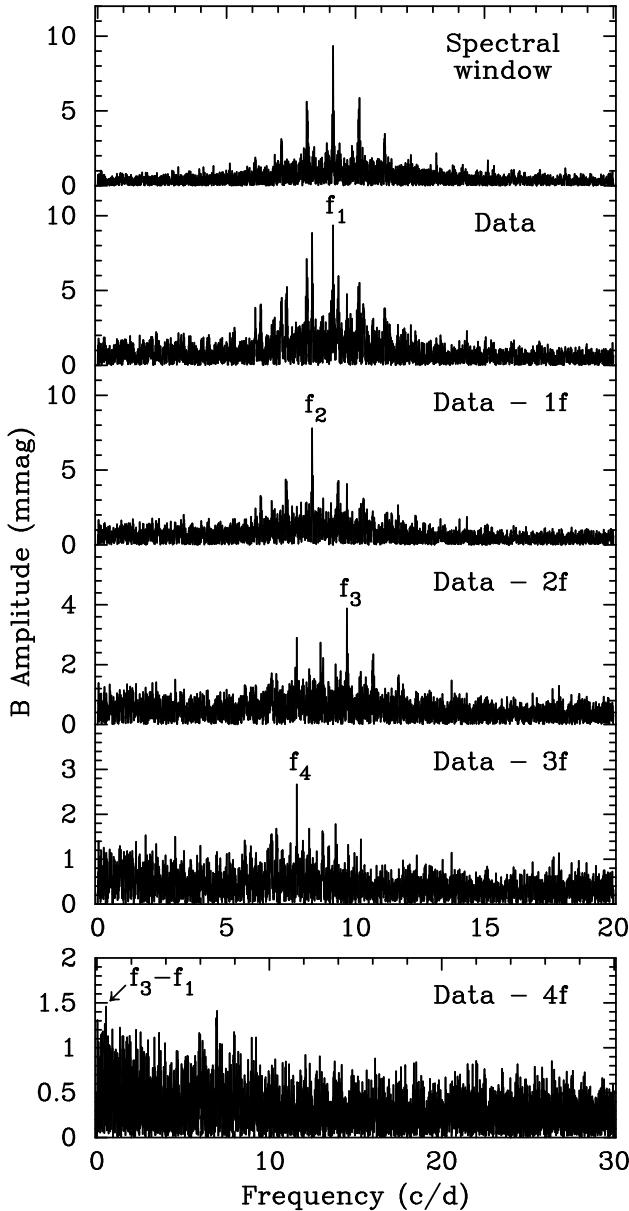


Figure 4. Spectral window and amplitude spectra of our B filter data of V433 Car. Some prewhitening steps of the detected frequencies are shown in consecutive panels. The lowest panel shows the amplitude spectrum of the combined UvBV residuals after all previously significant signals have been removed from the measurements. One combination frequency is detected that way.

we noted some additional low-frequency variability besides the pulsations of V433 Car. The differential light curves of HD 90434 relative to the comparison star for IL Vel, allowed us to identify HD 90434 unambiguously as a new variable. Figure 7 contains the spectral window and amplitude spectra of these data.

We detect one variation frequency for this star. Prewhitening it from the data, combining the residual light curves as done for the β Cephei stars, and computing the amplitude spectrum of this data set results in some evidence for additional variability (lowest panel of Fig. 7), but produces no more detections. The increase in noise level at

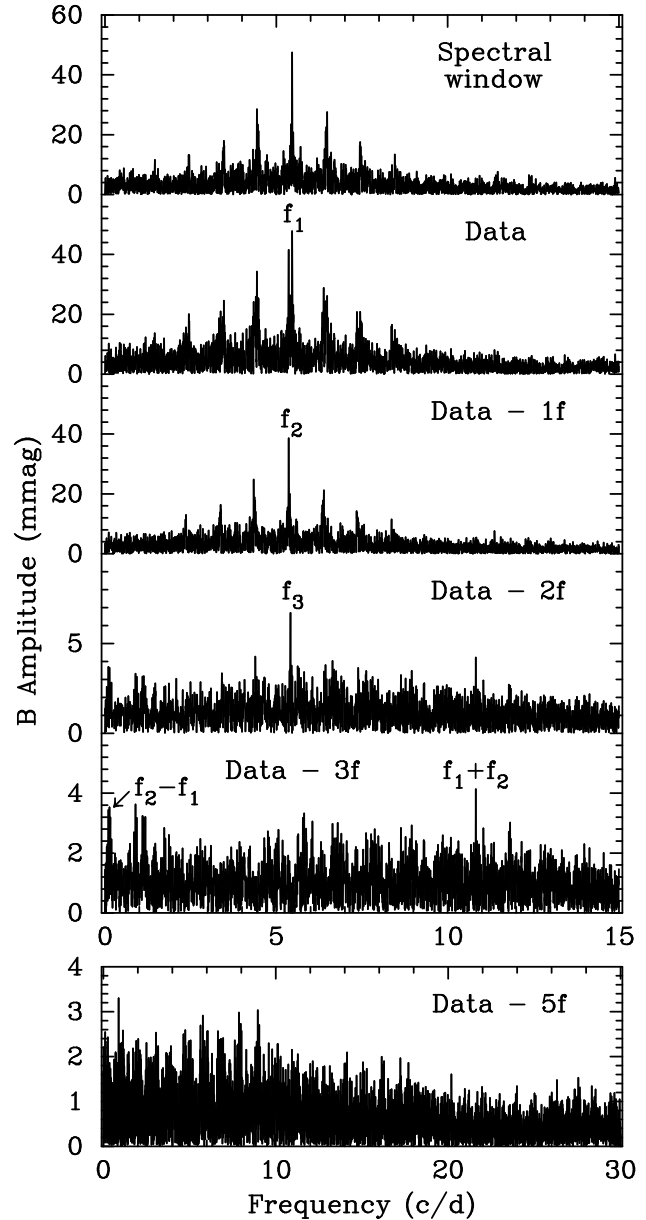


Figure 5. Spectral window and amplitude spectra of our B filter data of IL Vel. Some prewhitening steps of the detected frequencies are shown in consecutive panels. The lowest panel shows the amplitude spectrum of the combined UvBV residuals after all significant signals have been removed from the measurements.

low frequencies may however also (partly) be due to residual effects of extinction and sky transparency as the two stars are separated by about 10° in the sky. The frequency solution we derived for HD 90434 is given in Table 5. We note that the amplitude of the variability increases toward the blue, as confirmed by an examination for colour variations. No significant phase shifts between the light curves in the different filters were found.

3.4.2 HD 89768

After discovery of its variability, HD 90434 was replaced as a comparison star for V433 Car by HD 89768 whose spectral

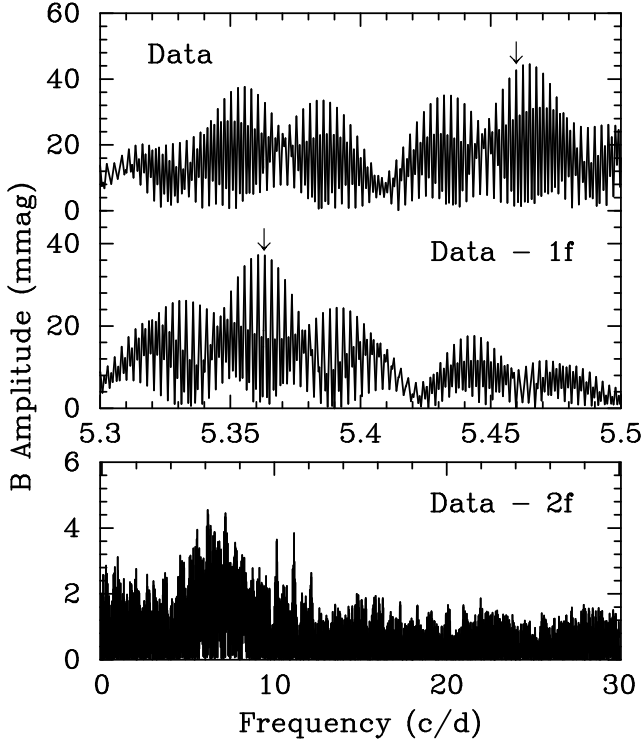


Figure 6. Amplitude spectra of Heynderickx & Haug’s (1994) B filter data of IL Vel; consecutive panels show some prewhitening steps. The positions of our frequencies f_1 and f_2 are indicated with arrows and adopted as definite for the prewhitening.

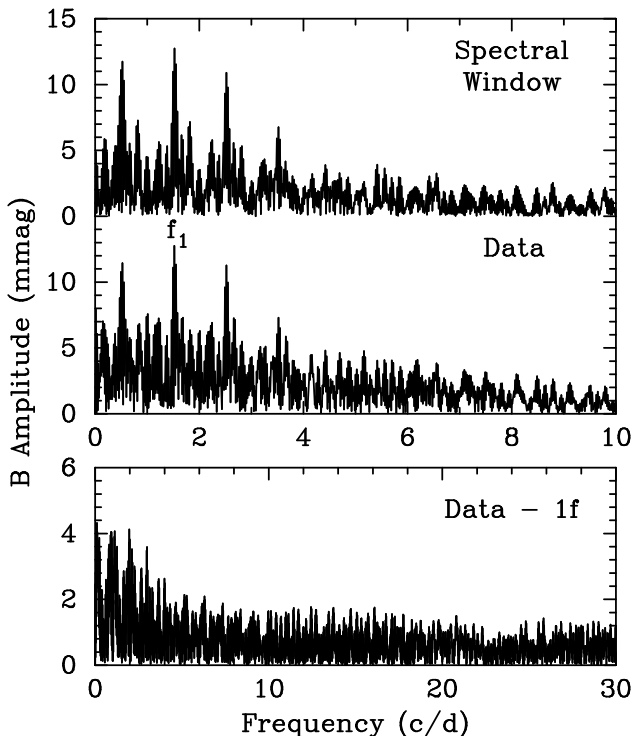


Figure 7. Upper two panels: spectral window and amplitude spectrum of our B filter data of HD 90434 relative to HD 79670. Lower panel: prewhitened amplitude spectrum of the combined residual light curves out to the Nyquist frequency.

Table 5. Results of the frequency analysis for the two comparison stars. Frequencies are mean values from results of all four filters weighted by the S/N ratio of the signal. Errors on the amplitudes were calculated with the formulae of Montgomery & O’Donoghue (1999). The S/N ratio quoted is the average of the values in the individual filters.

Star	HD 90434	HD 89768
Frequency (c/d)	1.5229 ± 0.0012	0.6875 ± 0.0004
U Amplitude (mmag)	15.9 ± 1.2	13.6 ± 1.2
B Amplitude (mmag)	11.5 ± 0.8	14.8 ± 0.6
V Amplitude (mmag)	9.2 ± 0.7	12.7 ± 0.5
v Amplitude (mmag)	11.4 ± 1.0	15.5 ± 0.9
Mean S/N	5.9	9.0

type of A1 IV/V places it outside any known pulsational instability region, but we were no luckier with this star. In fact, we only noticed that this object was variable as well when it was too late to replace it with yet another star.

We again constructed differential light curves with respect to HD 79670 and show its Fourier analysis in the same fashion as the one in the previous section in Fig. 8. Again, a single frequency suffices to explain the observed light variations, and some residual low-frequency variability seems present that we attribute to atmospheric effects. Table 5 contains our results for HD 89768 as well.

From the amplitudes in the different filters listed in Table 5 it appears that this star also shows some colour variability. We have therefore analysed the colour light curves as well, but we could not confirm this suspicion. It seems that the different amplitudes in the four filters are generated by noise effects and our errors are underestimates for variations at these low frequencies.

4 BASIC STELLAR PARAMETERS

4.1 The β Cephei stars

The astrophysical analysis of our results is facilitated by firstly restricting the physical parameter space occupied by these stars. Consequently, we have estimated their masses and temperatures with calibrations of multicolour photometry, as meaningful trigonometric parallaxes are not available. Fortunately, all three stars have already been measured in the Strömgen, Geneva and Johnson systems. We have retrieved the corresponding standard values from the Lausanne-Genève data base (<http://obswww.unige.ch/gcpd/gcpd.html>).

We have then applied different calibrations for effective temperature, surface gravity and absolute magnitude to the three stars. It seems important to use more than one calibration as their results often deviate. We can then hope to get a good average result with a realistic determination of its uncertainty. Absolute visual magnitudes were calculated from the Strömgen β index using Crawford’s (1978) results that also allow a determination of the interstellar reddening. We find $A_v = 0.90$ for IL Vel, $A_v = 0.38$ for V433 Car and $A_v = 1.24$ for KZ Mus.

We used the formulae by Napiwotzki, Schönberner & Wenske (1993) to calculate stellar temperatures from the

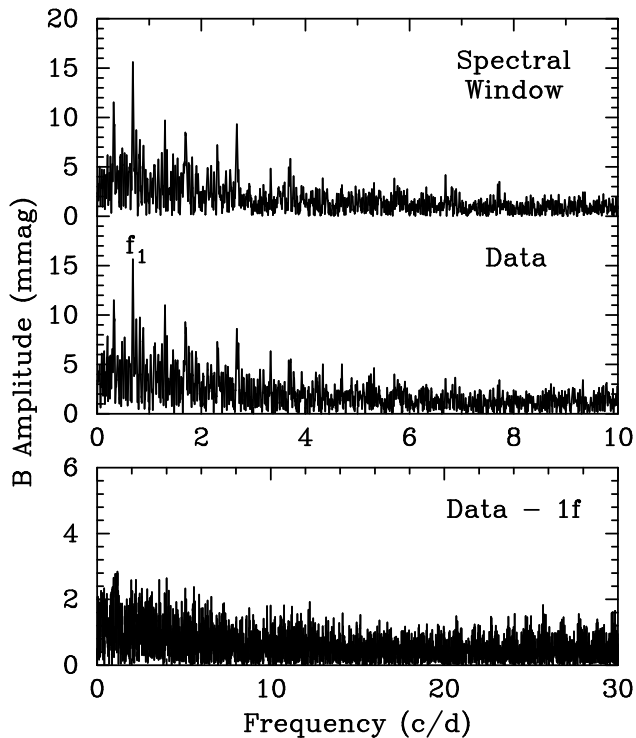


Figure 8. Upper two panels: spectral window and amplitude spectrum of our B filter data of HD 89768 relative to HD 79670. Lower panel: prewhitened amplitude spectrum of the combined residual light curves out to the Nyquist frequency.

Table 6. The adopted effective temperatures and luminosities for our target stars from standard photometry.

Parameter	IL Vel	V433 Car	KZ Mus
T_{eff} [kK]	23.6 ± 0.6	26.6 ± 0.7	26.0 ± 0.7
$\log L/L_{\odot}$	4.19 ± 0.22	4.20 ± 0.20	4.22 ± 0.20

Strömgen $[u - b]$ and $(b - y)_0$ indices as well as from Johnson $(B - V)_0$. The tables by Flower (1996) allow another temperature estimate from $(B - V)_0$ and also provide bolometric corrections. The latter were also determined from Drilling & Landolt’s (2000) tables. Estimates of the surface gravities of the three stars were obtained with the calibration by Smalley & Dworetzky (1995) from the Strömgen β index, including a correction proposed by Dziembowski & Jerzykiewicz (1999). Finally, we applied the work by Künzli et al. (1997) for the Geneva system that results in effective temperatures and surface gravities. Average values for the resulting effective temperatures and luminosities as well as error estimates are given in Table 6.

4.2 The variable comparison stars

The HIPPARCOS parallax of HD 90434 (ESA 1997) has a relative error that is too large to make it useful. The spectral classification and the Strömgen colours of the star imply it is a late B star. Johnson and Geneva colours of this object are also available at the Lausanne-Geneva data base. Con-

sequently, we applied the same calibrations that we have already used for the β Cephei stars to determine its effective temperature and luminosity. We derive $T_{\text{eff}} = 12.2 \pm 0.4$ kK and $\log L/L_{\odot} = 1.86 \pm 0.10$.

No standard photometry is available for HD 89768. However, from the mean magnitude differences of V433 Car from both of its comparison stars, we can estimate $(B - V) = 0.09$ and $(U - B) = 0.04$ for HD 89768. With the HIPPARCOS parallax of 2.09 ± 0.69 mas and the galactic reddening law by Chen et al. (1998), we can then estimate $(B - V)_0 = 0.01 \pm 0.03$ and $M_v = -0.7 \pm 0.9$. From the calibration by Napiwotzki et al. (1993) we then obtain $T_{\text{eff}} = 9250 \pm 400$ K, and the luminosity results in $\log L/L_{\odot} = 2.3 \pm 0.4$.

4.2.1 The nature of HD 90434 and HD 89768

The effective temperature and luminosity of HD 90434 as derived above put it into the instability region of the slowly pulsating B (SPB) stars (Dziembowski, Moskalik & Pamyatnykh 1993). The colour variability we found combined with the variation being in phase in the different filters supports this hypothesis and argues against an interpretation in terms of rotational modulation of a chemically peculiar star; the Strömgen m_1 index for HD 90434 does not suggest it is an Ap star either.

On the other hand, HD 89768 is not located in any known pulsational instability region, and we could not detect colour variability in its light curves. We suspect that the variability may be binary-induced, but spectroscopic data would be required to confirm our hypothesis.

5 MODE IDENTIFICATION

The ranges in effective temperature and luminosity of the β Cephei stars listed in Table 6 are an essential ingredient for mode identification. We have followed the method proposed by Balona & Evers (1999, see their paper for a detailed description). It uses theoretically calculated nonadiabatic parameters to determine the amplitude ratios between different wavebands that are the discriminator between the different modes of pulsation.

We computed stellar evolutionary models by means of the Warsaw-New Jersey evolution and pulsation code (described, for instance, by Pamyatnykh et al. 1998) for solar chemical composition. The models spanned a mass range between $8 - 16M_{\odot}$ in steps of $1M_{\odot}$. Guided by the projected rotational velocities of the stars listed in Table 1, we chose a rotational velocity of 100 km/s on the ZAMS for models representing IL Vel and KZ Mus, but 260 km/s for V433 Car. By comparing the model evolutionary tracks with the stellar parameters in Table 6, we inferred that IL Vel is a star with a mass between $10.5 - 13M_{\odot}$ in the second half of its main-sequence evolution, whereas KZ Mus and V433 Car are less evolved but somewhat more massive ($11.5M_{\odot} < M_* < 14M_{\odot}$).

We then proceeded by calculating theoretical UvBV amplitudes for all pulsationally unstable modes along model sequences that spanned the physical parameter space of our targets, whereby we extended the error bars in Table 6 by up to a factor of 2 to be conservative. We did not consider

the phase shifts between the different photometric bands because their measured relative error is much higher than that for amplitude ratios. We have not found phase shifts significant at the 3σ level and they have therefore no discriminative power.

The resulting theoretical amplitudes in the four passbands were normalised to that in the U filter, and the average amplitude ratio and its rms error were calculated. In this way we can also get an idea of the uncertainties involved in the calculation of theoretical results that need to be considered when being matched with the observations.

The comparison between the theoretical and observed colour amplitude ratios of IL Vel is shown in Fig. 9. We also include the UBV colour amplitude ratios from the data by Heynderickx & Haug (1984) with the correct frequencies f_1 and f_2 .

The identification for the two strongest modes of IL Vel is unambiguous: both have a spherical degree $\ell = 1$. The third pulsation mode we found that has a frequency intermediate between the other two is also nonradial and could be $\ell = 1, 2$ or 3 . Our mode identification is therefore consistent with that by Heynderickx et al. (1994), although they have used an incorrect alias and spurious frequencies.

Observed and theoretical amplitude ratios for the four modes of V433 Car are plotted in Fig. 10. The identifications we derive from that figure are not as clear as the ones for IL Vel. Mode f_1 is most likely $\ell = 2$, and the amplitude ratios for f_2 agree best with $\ell = 1$. All we can say about mode f_3 is that it is nonradial ($\ell = 2$ or $4?$), and mode f_4 may be $\ell = 0, 1, 2$ or 3 .

Heynderickx et al. (1994) arrived at similar conclusions concerning the identification of the modes of V433 Car, and they also reported inconsistencies of their identifications in different photometric systems. We must therefore consider the attempts to derive mode identifications for V433 Car as mostly inconclusive.

Turning now to KZ Mus, we show the comparison of its observed amplitude ratios with their theoretical predictions in Fig. 11. The identifications for the highest-amplitude modes of this star are very clear. The strongest mode of KZ Mus is quadrupole ($\ell = 2$), whereas mode f_2 is radial. This is in excellent agreement with the identification by Aerts (2000).

As we have a much larger data set available than Aerts (2000) did, we can also provide an identification for the third mode of KZ Mus, which is a dipole ($\ell = 1$). Only the identification for the weak fourth mode of this star does not point to an unambiguous spherical degree, but we can safely say that it is nonradial with $\ell \leq 3$; a radial identification is ruled out because this mode's frequency is too close to that of the radial mode f_2 .

Finally, we also look for a possible mode identification for our SPB candidate HD 90434. For this star, we adopted $3M_{\odot}$ models near the ZAMS guided by the results from Sect. 4.2 to determine the theoretical UvBV amplitude ratios. We then proceeded in the same manner as for the β Cephei stars, and present the comparison between theoretical and observed amplitude ratios in Fig. 12.

Modes of spherical degrees $\ell = 1$ and 4 give the best agreement, but $\ell = 2$ also seems a viable identification. The long period of the star and the normalisation of the amplitudes in the U band (where the absolute error on the ampli-

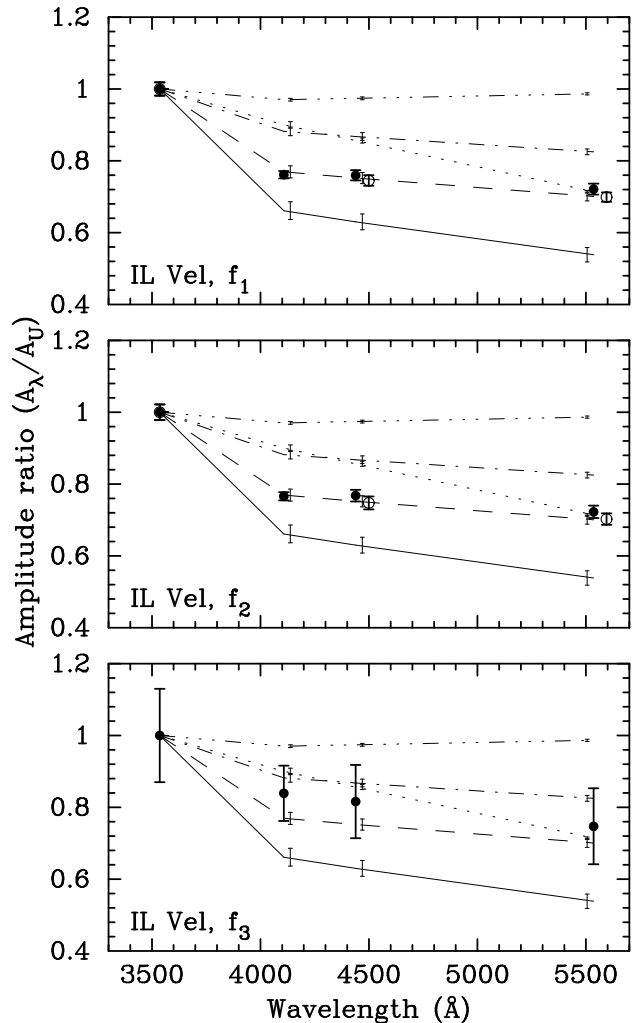


Figure 9. Observed and theoretical UvBV amplitude ratios (lines) for $0 \leq \ell \leq 4$ for IL Vel. Amplitudes are normalised at U. The filled circles with error bars are from our measurements, the open circles (somewhat shifted in wavelength for reasons of display) with error bars are for the data by Heynderickx & Haug (1984). The full lines are for radial modes, the dashed lines for dipole modes, the dashed-dotted lines for quadrupole modes, the dotted lines for modes of $\ell = 3$ and the dashed-dot-dot-dotted lines are for $\ell = 4$. The small error bars, also slightly shifted in wavelength, denote the uncertainty in the theoretical amplitude ratios. The upper panel is for mode f_1 , the middle one for f_2 , and the lower one for f_3 .

tude is largest) are suspected to result in larger systematic contributions to the observational errors than the formal values we adopted would include. Taking the effects of geometrical cancellation (Dziembowski 1977) into account, the most likely reason for the variability of HD 90434 is pulsation in a dipole mode.

6 ASTEROSEISMOLOGY

6.1 IL Vel

We will now take advantage of the information gathered in the previous sections to understand the pulsational be-

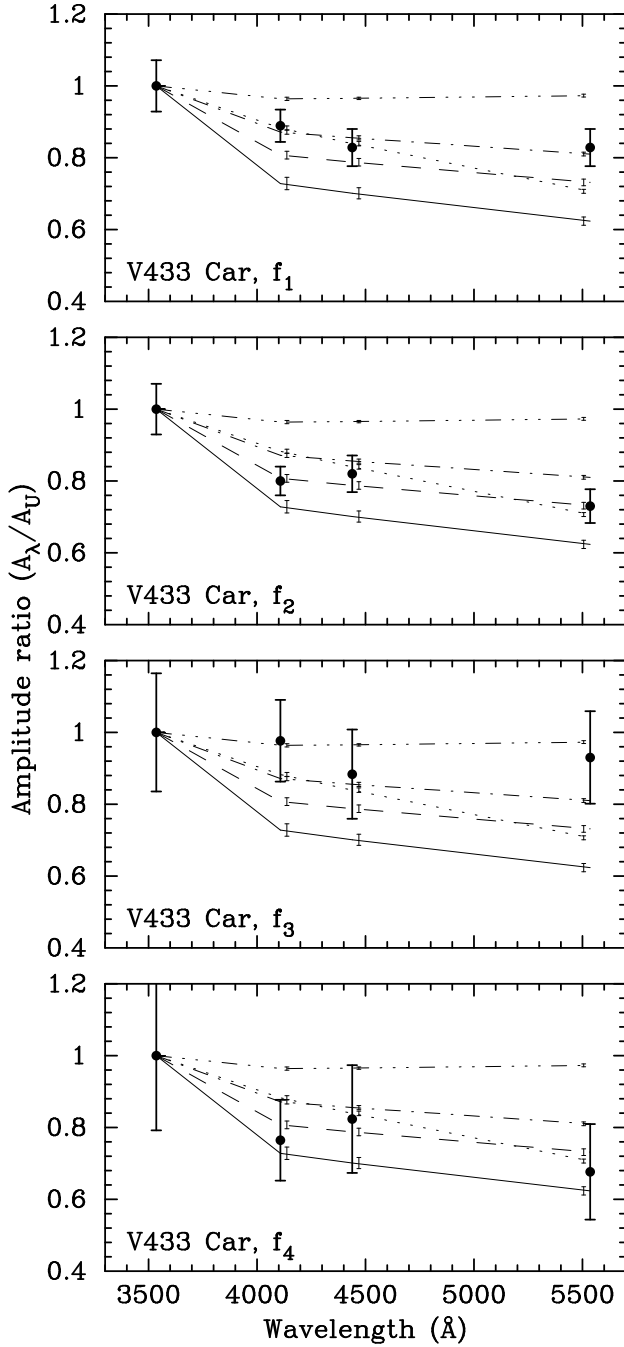


Figure 10. Observed (filled circles with error bars) and theoretical UvBV amplitude ratios (lines) for $0 \leq \ell \leq 4$ for V433 Car. Amplitudes are normalised at U. The full lines are for radial modes, the dashed lines for dipole modes, the dashed-dotted lines for quadrupole modes, the dotted lines for modes of $\ell = 3$ and the dashed-dot-dot-dotted lines are for $\ell = 4$. The small error bars somewhat shifted in wavelength denote the uncertainty in the theoretical amplitude ratios. The upper panel is for mode f_1 , the second for f_2 , the third for f_3 , and the lower one for f_4 .

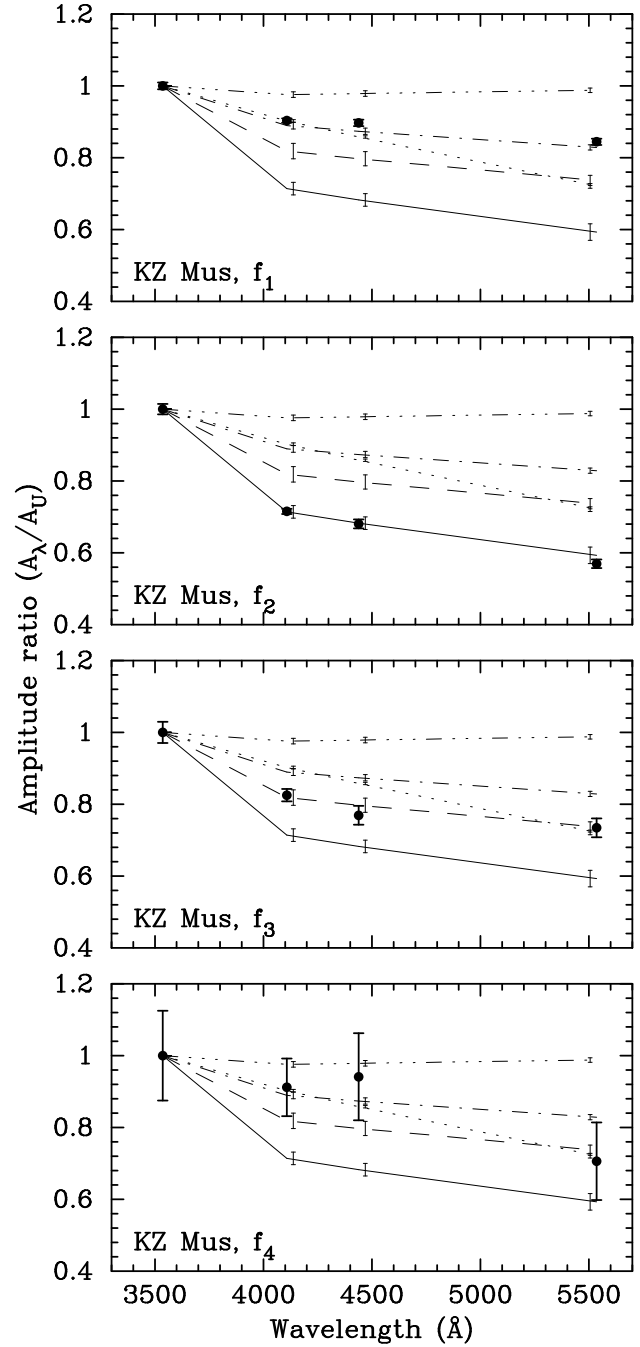


Figure 11. Observed (filled circles with error bars) and theoretical UvBV amplitude ratios (lines) for $0 \leq \ell \leq 4$ for KZ Mus. Amplitudes are normalised at U. The full lines are for radial modes, the dashed lines for dipole modes, the dashed-dotted lines for quadrupole modes, the dotted lines for modes of $\ell = 3$ and the dashed-dot-dot-dotted lines are for $\ell = 4$. The small error bars somewhat shifted in wavelength denote the uncertainty in the theoretical amplitude ratios. The upper panel is for mode f_1 , the second for f_2 , the third for f_3 , and the lower one for f_4 .

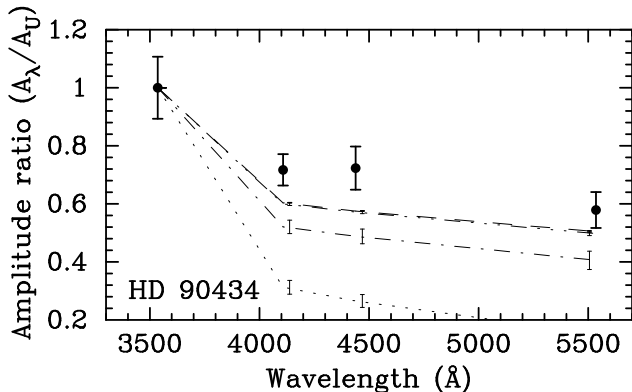


Figure 12. Observed (filled circles with error bars) and theoretical UvBV amplitude ratios (lines) for $1 \leq \ell \leq 4$ for HD 90434. Amplitudes are normalised at U. The dashed lines are for dipole modes, the dashed-dotted lines for quadrupole modes, the dotted lines for modes of $\ell = 3$ and the dashed-dot-dot-dotted lines are for $\ell = 4$. The small error bars somewhat shifted in wavelength denote the uncertainty in the theoretical amplitude ratios.

haviour of our three target stars by means of comparison with model calculations. We have again used the Warsaw-New Jersey stellar evolution and pulsation code for this part of the analysis. We note that we do not attempt an exhaustive seismic analysis of the stars because too few identified pulsation modes are available for such purposes. Instead, we want to determine what we can learn about the stars by means of standard models and procedures and we want to assess the potential for asteroseismology of β Cephei stars.

One tool that has been established for constraining the range of physical parameters of the seismological model of a star is stability analysis (see Pamyatnykh 2003 for a review). As a model of a pulsating star evolves, its radius changes, and the range of pulsationally unstable radial overtones of the eigenfrequencies varies as well. In conclusion, the frequency range of the unstable eigenmodes depends on the location of the model in the instability strip. This frequency range can then be matched with the one actually observed in the star.

Applying this method to IL Vel, we can take advantage of our mode identification. As all the modes for which we have a certain identification are $\ell = 1$, we can restrict the comparison to this single spherical degree only. Figure 13 shows evolutionary tracks for models between 8 and $16 M_{\odot}$ (we assumed solar chemical composition and a rotational velocity of 100 km/s on the ZAMS) in the theoretical HR diagram together with the parameters of the star from Table 6; models with a matching range of unstable frequencies are indicated.

Inspection of Fig. 13 shows very good agreement between the star's position in the HRD and the range of models that have the same frequency domain unstable. We note that the sequences of matching models sometimes have gaps as they evolve along the main sequence. This is due to a change in the type of modes that produce the match and their frequency evolution which is affected by avoided crossings. We caution that the strength of pulsational driving in β Cephei stars is strongly dependent on metal abundance (Moskalik & Dziembowski 1992, Pamyatnykh 1999). There-

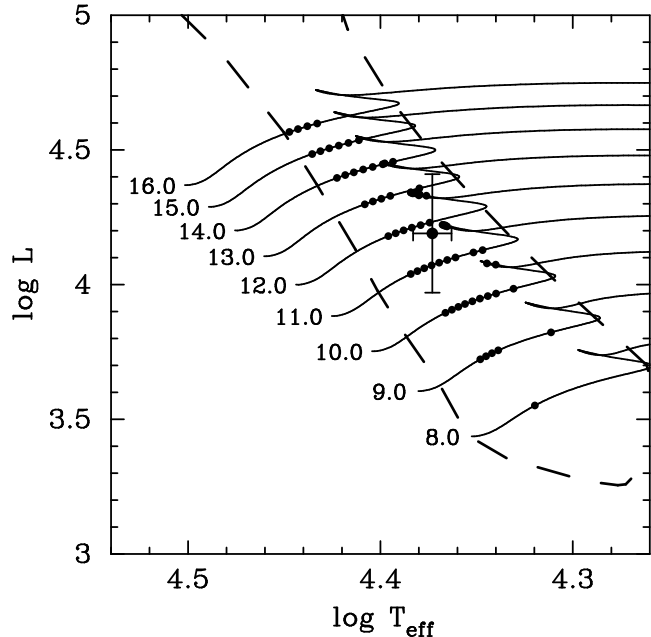


Figure 13. The position of IL Vel in the theoretical HR diagram. Some stellar model evolutionary tracks labeled with their masses (full lines) and the theoretical borders of the β Cephei star instability strip (Pamyatnykh 1999, dashed lines) are included for comparison. The sections of the evolutionary tracks that are marked with filled circles represent models in which the observed frequency range of the star is unstable.

fore the results in Fig. 13 are only an indication of the range of possible models for IL Vel.

The two $\ell = 1$ modes of IL Vel have similar frequencies; they are spaced by only 0.0986 c/d. The projected rotational velocity of the star ($v \sin i = 65$ km/s, cf. Table 1) implies a rotational period $P_{\text{rot}} < 5.8$ d for the star assuming a mass of $12 M_{\odot}$ as indicated by Fig. 13. At first glance, this suggests that those two modes cannot be caused by rotational splitting of a single mode. Three explanations for this close proximity of a p- and a g-mode. First, the star's pulsations are just undergoing an avoided crossing phenomenon (e.g. see Aizenman, Smeyers & Weigert 1976) resulting in a close proximity of a p- and a g-mode. Second, the two $\ell = 1$ modes are the central and prograde components of a multiplet, and the second-order rotational splitting is large enough to produce such a small frequency difference. Third, we may observe a gravity mode; the first-order rotational splitting of such a mode is approximately $\nu \approx (1 - (\ell(\ell + 1))^{-1})P_{\text{rot}}^{-1}$ (Winget et al. 1991).

We examine these hypotheses in Fig. 14, where we show the evolution of the rotational m -mode splitting and the frequencies of the $\ell = 1$ modes of a $12 M_{\odot}$ model with $v_{\text{rot,ZAMS}} = 70$ km/s along the main sequence. The first three pressure (p) and the first two gravity (g) modes are shown. From the upper panel of this figure it becomes clear that the observed frequency splitting of IL Vel can be easily reproduced by the model in the corresponding temperature range. In fact, this would be possible with models rotating as fast as 110 km/s. On the other hand, the rotational frequency splitting of any of these modes never becomes small enough that the observed frequency difference can be due to

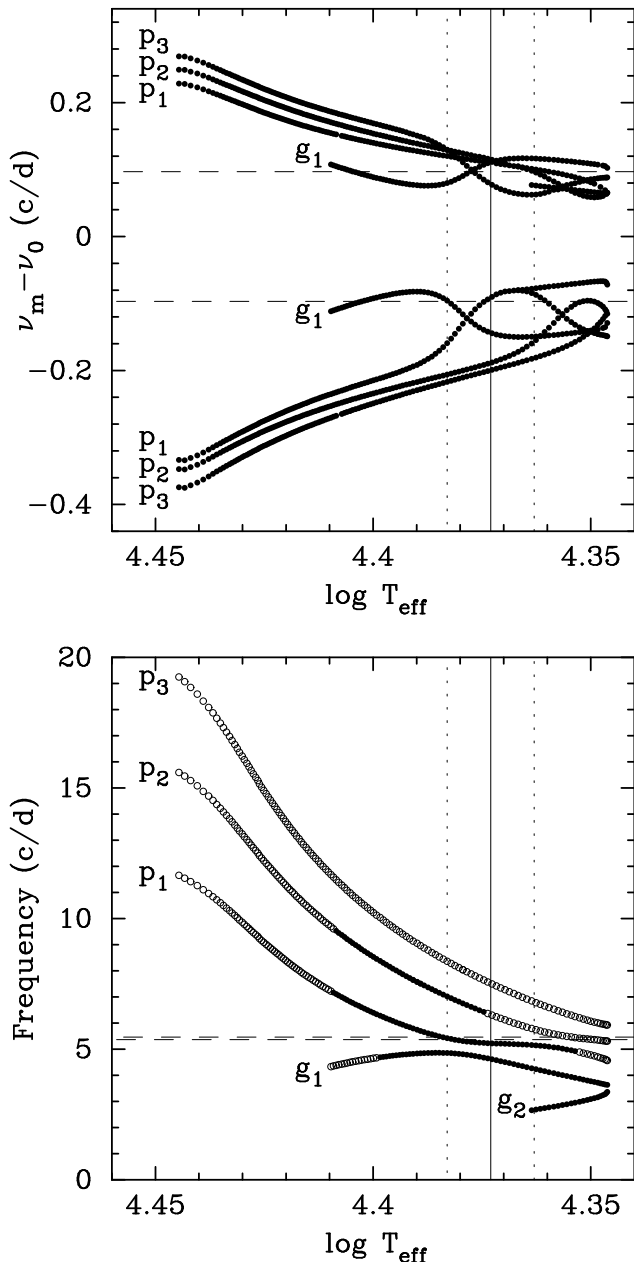


Figure 14. Upper panel: the size of rotational splitting for $\ell = 1$ modes of a $12 M_{\odot}$ model with $v_{\text{rot,ZAMS}} = 70 \text{ km/s}$ along its evolution along the main sequence. The first three p-modes and the first g-mode are indicated. The horizontal dashed lines denote the frequency difference between the two strongest modes of IL Vel, and the vertical solid line with parallel dotted lines is the effective temperature of the star and its error estimate from Table 6. Lower panel: stability and frequency evolution of $\ell = 1, m = 0$ mode frequencies in the same model. Modes that are pulsationally unstable are denoted with filled circles, the open circles are for stable modes. The two dashed lines represent the observed $\ell = 1$ frequencies, and the vertical lines again labels the effective temperature of the star and its error estimate. Note the avoided crossing of the p_1 and the g_1 mode starting at about $\log T_{\text{eff}} = 4.39$.

$\ell = 1$ modes of the same type and radial overtone but with $m = 1$ and $m = -1$. This also implies that the third mode of IL Vel cannot be another member of this multiplet.

To determine the modes that are potentially responsible for the pulsations of IL Vel, we have traced the frequencies of the individual $\ell = 1$ modes of the same model as used before along the main sequence in the lower panel of Fig. 14. The mode originating as p_1 on the ZAMS has a frequency very similar to the two observed for IL Vel over the whole temperature range estimated for the star, and is unstable as well. This mode has already undergone an avoided crossing with the g_1 mode and should therefore also have gravity mode characteristics, i.e. it is a mixed mode. In higher-mass models, dipole modes at this frequency become stable against pulsations, and in models below $11 M_{\odot}$ the g_1 mode reproduces the observed frequency in the temperature range appropriate for IL Vel.

Another observation from Fig. 14 is that the p_1 and g_1 modes never come closer together than about 0.5 c/d . It is therefore unlikely that the two modes observed in IL Vel originate from different modes that just happen to undergo an avoided crossing. If we consider the hypothesis that the proximity of the two observed $\ell = 1$ modes is caused by the effects of second-order rotational splitting, we find that $v_{\text{rot}} \gtrsim 160 \text{ km/s}$, and hence $i < 25^\circ$, which is also unlikely. In addition, the high amplitude of the prograde mode and the absence of the retrograde component of the hypothesised triplet would also be difficult to explain.

We conclude that the two dipole pulsation modes of IL Vel are most likely due to rotationally split components of the mode originating as p_1 on the ZAMS. One of these modes is $m = 0$, the other one $|m| = 1$, and $65 \text{ km/s} < v_{\text{rot}} < 110 \text{ km/s}$.

6.2 V433 Car

We have performed a similar analysis for V433 Car. Regrettably, we could not obtain unambiguous ℓ identifications for any of its modes. On the other hand, the excited frequency range of the star is larger, which may however be related to it being a fast rotator. In any case, we show the match of unstable model frequencies to that of the observed ones in Fig. 15. The model evolutionary tracks are again for solar chemical composition, but for a rotational velocity of 260 km/s on the ZAMS, and we considered all modes with $0 \leq \ell \leq 4$.

Again, the agreement between theory and observation is fairly good, even when keeping in mind that our analysis does not take the frequency spread due to fast rotation of the star. However, as the observational results only allow us a rough qualitative comparison between observations and theory for V433 Car, this is not regarded as being important. V433 Car appears to be an object of about $13 M_{\odot}$ that has just entered the β Cephei star instability strip.

6.3 KZ Mus

The asteroseismological prospects of KZ Mus appear much better. In particular, we have unambiguously identified one of its modes as radial, and two more modes also have unique ℓ assignments. In the same fashion as in the previous sections, we show model evolutionary tracks (for $v_{\text{rot,ZAMS}} =$

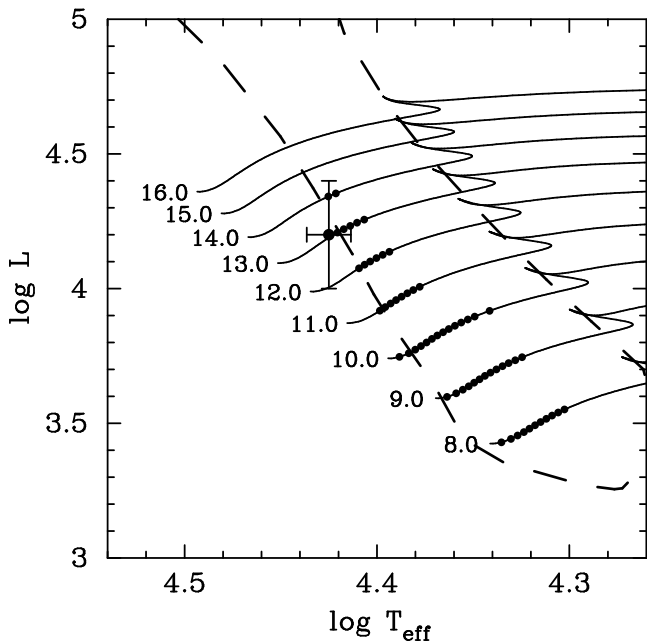


Figure 15. The position of V433 Car in the theoretical HR diagram. Some stellar model evolutionary tracks labeled with their masses (full lines) and the theoretical borders of the β Cephei star instability strip (Pamyatnykh 1999, dashed lines) are included for comparison. The sections of the evolutionary tracks that are marked with filled circles represent models in which the observed frequency range of the star is unstable. For some models, we obtain unstable pulsation modes somewhat outside the blue edge of the theoretical instability strip, which is due to $\ell = 4$ modes; the borders indicated are only for $\ell \leq 2$.

100 km/s) in the theoretical HR diagram, the star's position in it, and models with unstable modes in the observed frequency range in Fig. 16. In addition, we have indicated the locations of models that have a radial mode at 5.9506 c/d as observed for KZ Mus.

As for the other two stars, we find no disagreement between models with unstable modes in the observed frequency range and the observationally determined position of the star in the HRD. Figure 16 also allows us to reject the second overtone as the identification for the radial mode of KZ Mus, as it is inconsistent with the star's evolutionary state, and it never becomes pulsationally unstable.

However, we cannot say at this point whether the radial mode is the fundamental or first overtone. Models with the fundamental radial mode at 5.9506 c/d are in better agreement with the stellar parameters from Table 6, but it may be stable in models with the mass inferred for the star. On the other hand, for this mode to be the first overtone, only models at the upper limits on mass and luminosity seem appropriate.

We attempted to find further constraints on the parameter space occupied by KZ Mus by using the nonradial modes that we identified unambiguously; any model representing the star should have modes of the same ℓ in the correct frequency range. All models with the radial fundamental or first overtone mode at 5.9506 c/d that we investigated could be used to reproduce the observed nonradial modes given the unknown angular rotational velocity of the star. However, when imposing mode stability as an addi-

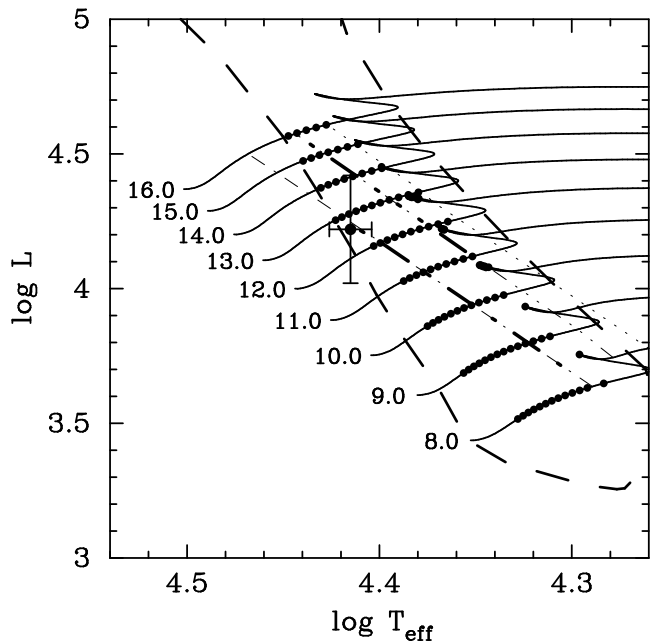


Figure 16. The position of KZ Mus in the theoretical HR diagram. Some stellar evolutionary tracks labeled with their masses (full lines) and the theoretical borders of the β Cephei star instability strip (Pamyatnykh 1999, dashed lines) are included for comparison. The sections of the evolutionary tracks that are marked with filled circles represent models in which the observed frequency range of the star is unstable. The lines going from the top left to the bottom right are locations of models that have a radial mode at 5.9506 c/d. For models on the dashed-dotted line this would be the fundamental radial mode, those connected by the dotted line show the first overtone at this frequency, and the ones connected by the dashed-dot-dot-dotted line have their second radial overtone at 5.9506 c/d. The thick parts of these lines connect the models which are pulsationally unstable.

tional criterion, it is found that model sequences of 12 and 13 M_{\odot} give best agreement with the observations.

In this case, it is most likely that f_2 is the radial fundamental mode of KZ Mus. Then the $\ell = 1$ mode would be associated with the mode originating as p_1 at the ZAMS and the observed $\ell = 2$ most likely corresponds to the mode originating as g_1 .

7 SUMMARY, DISCUSSION AND CONCLUSIONS

In an attempt to investigate the asteroseismological potential of the β Cephei stars, we have obtained 127 – 150 h of differential photoelectric photometry for each of the three pulsators IL Vel, V433 Car and KZ Mus. In line with the recent results by Stankov et al. (2002) and Cuypers et al. (2002), we have shown that low-amplitude pulsation modes are present in β Cephei stars, and that large observational efforts to determine their mode spectra in detail are justified. We therefore confirm the importance of β Cephei stars as asteroseismological targets for both ground and space based measurements.

By using the amplitude ratios of the different pulsation modes in the UvBV filters of the Johnson and Strömgren

systems, we performed mode identification. We obtained unambiguous results for all pulsation modes with photometric amplitudes larger than about 10 mmag in V, or with relative errors on their amplitude smaller than 3%. The modes we could identify were the two dominant ones of IL Vel and the three strongest of KZ Mus, but none of V433 Car.

This may not only be due to its photometric amplitudes that are small compared to those of the other two β Cephei stars. We have shown that V433 Car is a fast rotator, and therefore mode coupling (see Daszyńska-Daszkiewicz et al. 2002 and references therein) may occur. Mode coupling affects the predicted colour amplitude ratios and phase shifts. Since we have not taken this into account in our analysis, it may be at least partly responsible for the ambiguous mode identifications for this star.

On the other hand, our results for the more slowly rotating stars appear reliable, which represents a good motivation for studying a larger number of multiperiodic β Cephei stars in the future. Our limit of the relative error of 3% of the photometric amplitudes for successful mode identification can then serve as a guideline for planning future campaigns.

We have performed model calculations for our three targets. The outcome was also quite encouraging. Although we only detected up to four modes per star (thus our observational constraints on the models are not very strong), in no case disagreements between the observational results and model predictions were found. The observationally determined positions of the stars in the HR diagram could be reproduced by models that have the same range in pulsation frequencies unstable as are excited in the real stars.

In addition, we were able to place constraints on the types of mode observed in IL Vel and KZ Mus. We have shown that the most likely explanation for the two dipole modes of IL Vel are rotationally split components (one necessarily being $m = 0$) of the mode originating as p_1 on the ZAMS. The third mode of IL Vel cannot be another multiplet member, and the equatorial rotational velocity of the star must be smaller than 110 km/s. If the radial mode observed in KZ Mus is the fundamental, then the high-amplitude $\ell = 2$ mode is most likely the one originating as g_1 , and the $\ell = 1$ mode we identified is probably the one originating as p_1 .

We cannot push the asteroseismological analysis of the three stars further at this point because too few modes have been detected and identified for detailed modelling. However, we strongly suspect that more modes are present in IL Vel that just need better time resolution to be detected. KZ Mus may have more modes as well, and a unique mode identification for its fourth mode may place a constraint on the star's rotation frequency. Further work on both stars should also include time-resolved spectroscopic observations to determine the azimuthal order m of the high-amplitude nonradial modes; although both objects are $V \approx 9.1$, the spectra we obtained suggests this is possible. Determinations of the metal abundances of the stars would also be a valuable ingredient for model calculations. With all these observations in hand, precision asteroseismological studies of IL Vel and KZ Mus appear possible.

ACKNOWLEDGEMENTS

This work has been supported by the Austrian Fonds zur Förderung der wissenschaftlichen Forschung under grant R12 to GH and by travel support for FR and TT under grant P14546-PHY. We thank Wolfgang Zima for helping with some of the observations. GH is indebted to Alosha Pamyatnykh for helpful discussions, for providing theoretical instability domains for the β Cephei stars and to him and Anamarija Stankov for comments on a draft version of this paper. This research has made use of the SIMBAD and Vizier databases, operated at CDS, Strasbourg, France and the GCPD database, operated at the Institute of Astronomy of the University of Lausanne.

REFERENCES

- Aerts C., 2000, *A&A* 361, 245
 Aizenman M., Smeyers P., Weigert A., 1976, *A&A* 58, 41
 Balona L. A., Evers E. A., 1999, *MNRAS* 302, 349
 Breger M., et al., 1993, *A&A* 271, 482
 Chen, B., Vergely, J.L., Valette, B., Carraro, G. 1998, *A&A*, 336, 137
 Crawford D. L., 1978, *AJ* 83, 48
 Cuypers J., Aerts C., Buzasi D., Catanzarite J., Conrow T., Laher R., 2002, *A&A* 392, 599
 Daszyńska-Daszkiewicz J., Dziembowski W. A., Pamyatnykh A. A., Goupil M.-J., 2002, *A&A* 392, 151
 Drilling J. S., Landolt A. U., 2000, in *Allen's Astrophysical Quantities*, 4th edition, ed. A. N. Cox, Springer Verlag, p. 392
 Dziembowski W. A., 1977, *Acta Astr.* 27, 203
 Dziembowski W. A., Moskalik P., Pamyatnykh A. A., 1993, *MNRAS* 265, 588
 Dziembowski W. A., Jerzykiewicz M., 1999, *A&A* 341, 480
 ESA, 1997, *The Hipparcos and Tycho catalogues*, ESA SP-1200
 Flower P. J., 1996, *ApJ* 469, 355
 Gray R.O., Corbally C.J., 1994, *AJ* 107, 742
 Heynderickx D., 1992, *A&AS* 96, 207
 Heynderickx D., Haug U., 1994, *A&AS* 106, 79
 Heynderickx D., Waelkens C., Smeyers P., 1994, *A&AS* 105, 447
 Houk N., Cowley A. P., 1975, *Michigan Spectral Catalogue*, Vol. 1
 Künzli M., North P., Kurucz R. L., Nicolet B., 1997, *A&AS* 122, 51
 Lampens P., 1988, PhD dissertation, Katholieke Universiteit Leuven, Belgium
 Montgomery M. H., O'Donoghue D., 1999, *Delta Scuti Star Newsletter* 13, 28 (University of Vienna)
 Moskalik P., Dziembowski W. A., 1992, *A&A* 256, L5
 Napiwotzki R., Schönberner D., Wenske V., 1993, *A&A* 268, 653
 Pamyatnykh A. A., 1999, *Acta Astr.* 49, 119
 Pamyatnykh A. A., 2003, in *Asteroseismology Across the HR Diagram*, ed. M. J. Thompson, M. S. Cunha, M. J. P. F. G. Monteiro, Kluwer, in press
 Pamyatnykh A. A., Dziembowski W. A., Handler G., Pikal H., 1998, *A&A* 333, 141
 Smalley B., Dworetzky M. M., 1995, *A&A* 293, 446
 Soufi F., Goupil M. J., Dziembowski W. A., 1998, *A&A* 334, 911
 Sperl M., 1998, Master's Thesis, University of Vienna
 Stankov A., Handler G., Hempel M., Mittermayer P., 2002, *MNRAS* 336, 189
 Waelkens C., Aerts C., Kestens E., Grenon M., Eyer L., 1998, *A&A* 330, 215
 Winget D. E., et al., 1991, *ApJ* 378, 326